Supplementary Information for "Multitype topological transitions and multichannel directional topological photonic routings in chiral metamaterials"

Ning Han[1*], Mingzhu Li[2†], Yilin Zhang[1], Rui Zhao[3††], Fujia Chen[3], Lu Qi[4], Chenxia Li[1], and Shutian Liu[5]

1. *College of Optical and Electronic Technology, China Jiliang University, Hangzhou 310018, China*
2. *School of Information and Electrical Engineering, Hangzhou City University, Hangzhou 310015, China*
3. *State Key Laboratory of Extreme Photonics and Instrumentation, ZJU-Hangzhou Global Scientific and Technological Innovation Center, Zhejiang University, Hangzhou 310027, China*
4. *School of Physical Science and Technology, Yangzhou University, Yangzhou 225002, China*
5. *School of Physics, Harbin Institute of Technology, Harbin 150001, China*

[*] ninghan@cjlu.edu.cn

[†]limz@hzcu.edu.cn

[††]ruizhao@zju.edu.cn

This PDF file includes:

Supplementary Text

Supplementary Note 1 to Note 5

Figs. S1 to S5

Supplementary Note 1. Chiral photonic metamaterial design.

In general, the metal helical structure is a universal scheme for achieving the magnetoelectric coupling effect γ [16, 35, 37, 45]. Here, following the ideas of Refs. [35, 45], we show the schematic view of the metallic structure we discussed in Eq. (1) [see Figs. S1(a) and S1(b)]. Similar to Ref. [35], the unit cell in Fig. S1(a) is constructed by stacking a tri-layer medium (1-3). In particular, to obtain the desired hyperbolic response of ε_z in Eq. (1), a metallic wire is formed along the z-direction on the top layer 1. In Fig. S1(a), a metal helix in the bottom layer 3 is oriented along the y-direction, where an electric field along the y-direction can generate helical current along the metal structures, which forms a magnetic dipole moment along the y-direction as well [45]. In this case, the chirality term γ in Eq. (1) arises. Moreover, the blank layer 2 between the top and bottom layer can be designed to avoid shorting contact between them.

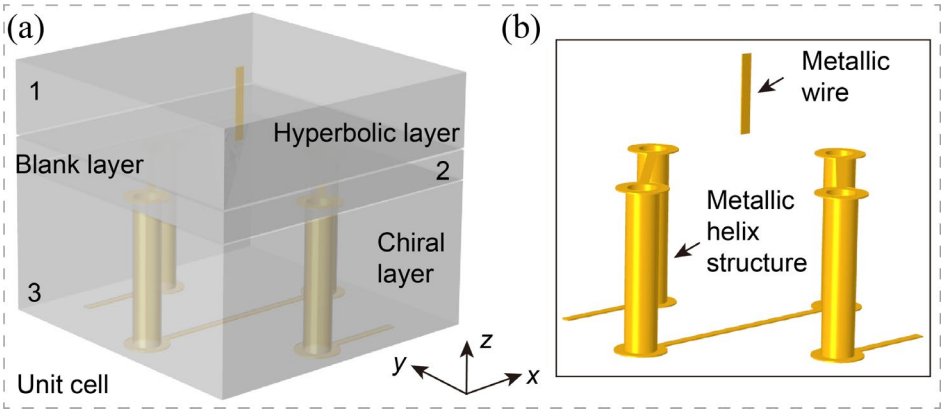

Fig. S1. (a), (b) Schematic view of the metallic structure of the chiral metamaterials we discussed in Eq. (1). For improved visibility, the dielectric FR4 [see gray part in (a)] in (b) has been removed.

Supplementary Note 2. 2D dispersion lines ω(k_z) at fixed k_y for Fig. 1(d).

Here, based on Eq. (4), we show the 2D dispersion lines ω(k_z) at fixed k_y of the low-frequency negative chirality Weyl points [see Fig. 1(d)], as illustrated in Fig. S2(a). Here, similar to Fig. 1(e) [or see Fig. S2(b)], the 2D branch crossings associated with the low-frequency Weyl points occur only when k_y=ω$_1$=0.549242 [see Eq. (6)], as indicated by the green lines in Fig. S2(b).

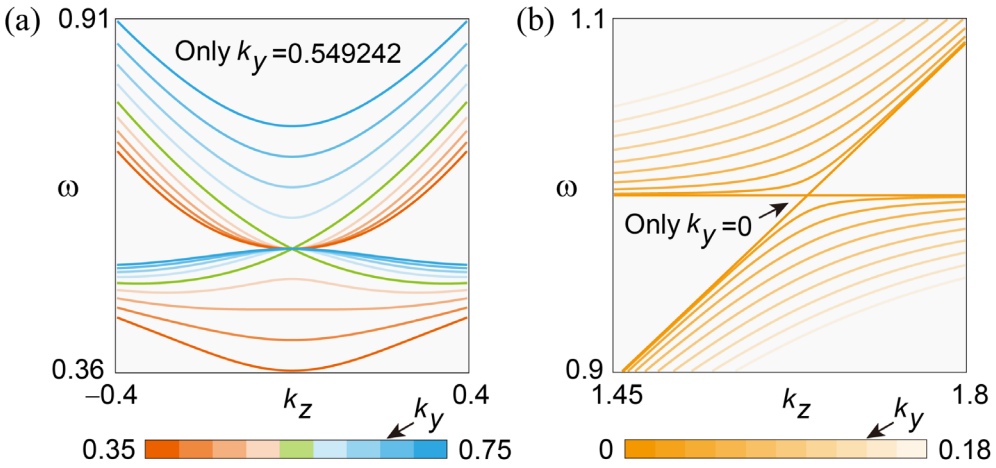

Fig. S2. (a), (b) The 2D dispersion lines ω(k_z) at fixed k_y of the low-frequency negative and high-frequency positive chirality Weyl points in Fig. 1(a), respectively.

Supplementary Note 3. 3D equifrequency surfaces under different angular frequencies ω in the phase I region.

In Fig. S3, when the angular frequencies ω are located in the phase I region ($0<\omega<\omega_0=0.3$), similar to Fig. 2(c), there is always mixed-type dispersion containing twofold type-I hyperboloid (orange) and an ellipsoid (pink) 3D equifrequency surfaces along the z-direction of the chiral metamaterials. Moreover, the 3D hyperboloid and ellipsoid equifrequency surfaces can always maintain a well separation in momentum space, i.e., the stable band gaps can be formed in the k_z direction [see Fig. S3]. Therefore, the 3D equifrequency surfaces of the phase I region of the comprehensive topological phase diagram [see Fig. 2(a)] are consistent.

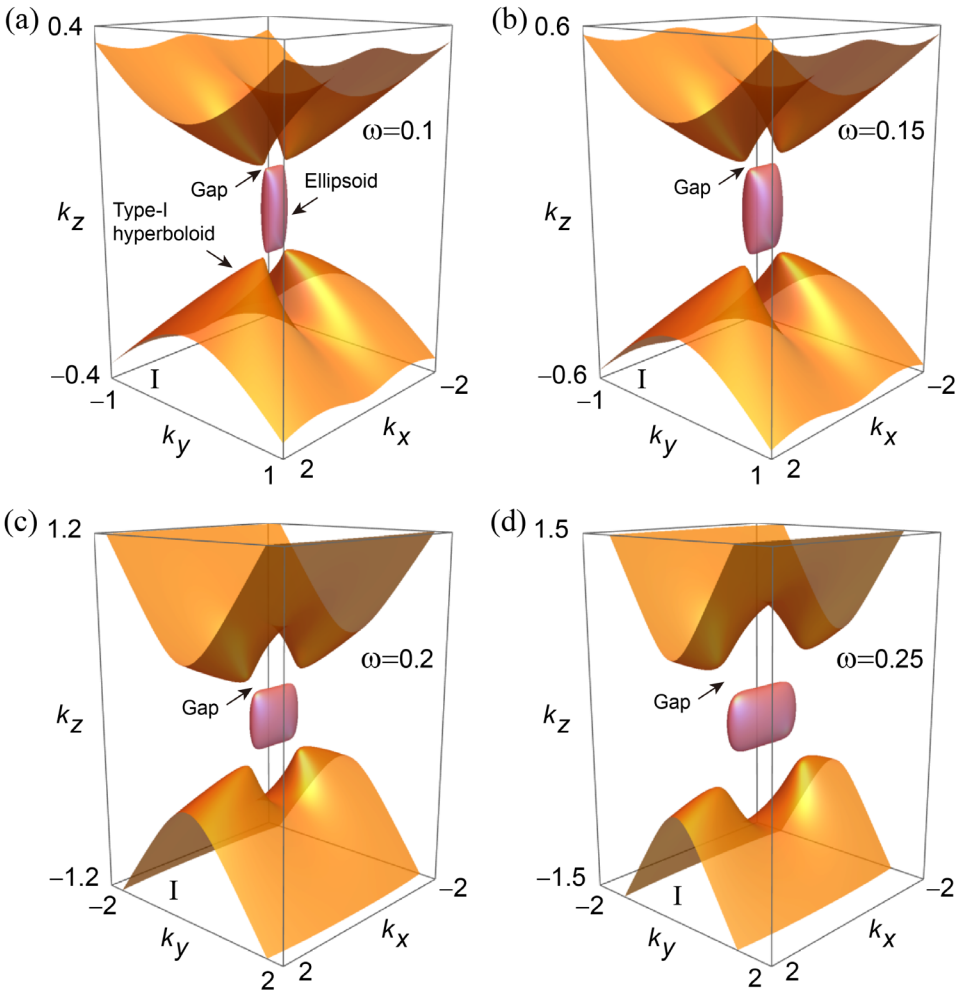

Fig. S3. (a)-(d) The 3D equifrequency surfaces of the phase I [see Fig. 2(a)] region at different angular frequencies ω.

Supplementary Note 4. The band gap shown in Fig. 5(i) would disappear when the angular frequency ω is less than the low-frequency Weyl points ω_1.

In the phase III region, the 2D equifrequency lines are the ellipsoid (light-red) and twofold type-I hyperboloid (orange) mixed type, as shown in Fig. S4(a) and Figs. 5(c)-(f). In this case, the 2D equifrequency lines of chiral metamaterials and vacuum states have complete band gaps, as illustrated by the light-purple regions in Fig. S4(a). However, once the angular frequency ω is located in the phase II region, i.e., ω is less than the low-frequency Weyl points ω_1, the complete band gap in the z-axis direction in Fig. S4(a) disappears, as illustrated in Fig. S4(c). Thus, in Fig. 5(i), the k_z band gap disappears when the angular frequency ω is less than ω_1 (0.549242).

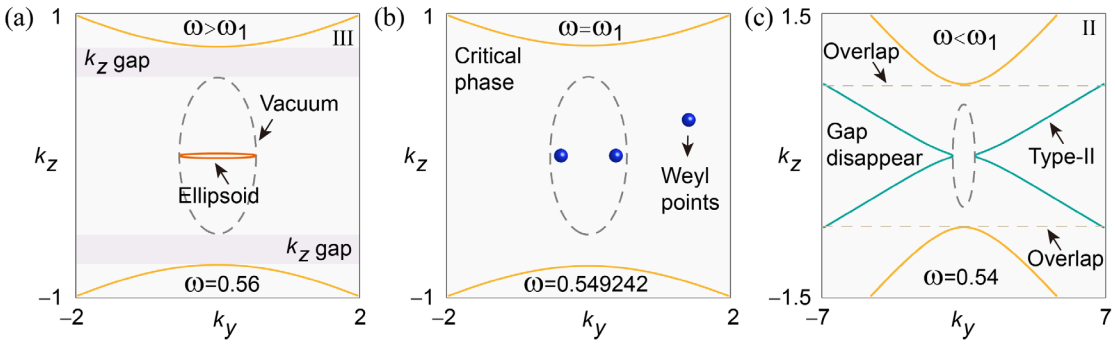

Fig. S4 (a)-(c) The multiple (from complete k_z gap to gap disappear case) 2D equifrequency lines caused by the evolution of parameters ω. They correspond to different phase III, critical phase, and phase II regions in Fig. 2(a), respectively.

Supplementary Note 5. The cladding-free topological surface waves are caused by the high-local surface states of common gap regions.

Here, we take Fig. 6(a) as an example to analyze the mechanism of implementing topological surface waves without cladding structures. In Fig. S5(a), the surface states of chiral metamaterials and vacuum states exist in common band gaps, as shown by the shadow regions. Moreover, we show the intensity of the surface state (such as point D) diminishes sharply as it extends away from the boundary (the skin depth x/λ in the vacuum state side is 0.53), indicating a high-local characteristic [see Fig. S5(b)]. Thus, the surface wave in Fig. 6(a) can directly meet the topological protection transmission at the vacuum interface, getting rid of the dependence on the cladding structure.

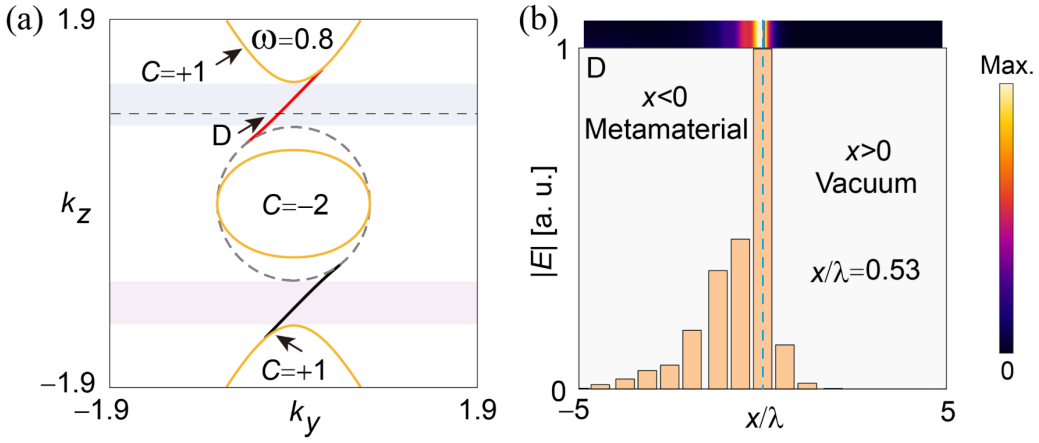

Fig. S5 (a) 2D equifrequency lines of the bulk states and Fermi arc surface states when angle frequency ω=0.8. It corresponds to Fig. 5(e) in the manuscript. (b) Mode profiles $|E|$ and numerical simulation of high-local surface states of the gap mode D in (a).